

# Quantum-confinement effects on the optical and dielectric properties for mesocrystals of BaTiO<sub>3</sub> and SrBi<sub>2</sub>Ta<sub>2</sub>O<sub>9</sub>

Shigemi Kohiki,<sup>a)</sup> Syozo Takada, Akihiko Shimizu, Kenichi Yamada, and Hiroataka Higashijima

*Department of Materials Science, Kyusyu Institute of Technology, Tobata, Kita-kyusyu 804-8550, Japan*

Masanori Mitome

*National Institute for Research in Inorganic Materials, Tsukuba, Ibaraki 305-0044, Japan*

(Received 25 June 1999; accepted for publication 29 September 1999)

We present optical and dielectric quantum-confinement effects for mesocrystals smaller than 30 Å of BaTiO<sub>3</sub> and SrBi<sub>2</sub>Ta<sub>2</sub>O<sub>9</sub> in uniform mesopores of the MCM-41 molecular sieve. For BaTiO<sub>3</sub> mesocrystals we observed a blueshift in optical absorption edge from 3.0<sub>2</sub> to 3.3<sub>5</sub> eV, and a decrease in dielectric constant maximum temperature from 130 to 55 °C. For SrBi<sub>2</sub>Ta<sub>2</sub>O<sub>9</sub> mesocrystals we also observed an increase in the optical absorption edge from 2.7<sub>0</sub> to 4.1<sub>8</sub> eV, and a decrease in the dielectric constant maximum temperature from 320 to 180 °C. The observed optical and dielectric quantum-confinement effects generally agree with the recognized consequence of reduced size. © 2000 American Institute of Physics. [S0021-8979(00)08601-1]

## I. INTRODUCTION

Size effects have been of great interest in the science and technology of ferroelectrics.<sup>1</sup> Reported ferroelectric critical size (the size at which ferroelectricity disappears) of BaTiO<sub>3</sub> particles varies from 100 to 1000 Å.<sup>2-6</sup> There are disagreements between the reported critical sizes. The disagreement may result from significant differences in both size and size distribution of the samples. These should depend on processing methods and conditions. And, additional effects by grain boundaries and/or internal stress should complicate the experimental results. Furthermore, the grains or particles in the reported critical size experiments were not sufficiently small to discuss the quantum size effect.

In this article we report blueshifts of the optical absorption edge, and decreases in the dielectric constant maximum temperature for mesocrystals  $\leq 30$  Å of BaTiO<sub>3</sub> and SrBi<sub>2</sub>Ta<sub>2</sub>O<sub>9</sub>, perovskite-based ferroelectrics, in the mesopores of MCM-41 molecular sieve. It is well known that the mesoporous silicate MCM-41 has uniform columnar periodic hexagonal pores ranging from 15 to 100 Å and separated by 8 to 9 Å walls.<sup>7</sup> BaTiO<sub>3</sub> is a typical ferroelectric material for optoelectronic devices with the pseudoisotropic perovskite structure ( $a=3.9920$ ,  $b/a=1.000$ , and  $c=4.0361$  Å),<sup>8</sup> and SrBi<sub>2</sub>Ta<sub>2</sub>O<sub>9</sub> is a promising material for ferroelectric random access memory devices<sup>9</sup> with an anisotropic crystal structure ( $a=5.512$ ,  $b/a=1.000$ , and  $c=25.00$  Å).<sup>10</sup> SrBi<sub>2</sub>Ta<sub>2</sub>O<sub>9</sub> consists of both Sr-Ta-O perovskite blocks and Bi<sub>2</sub>O<sub>2</sub> layers. It is expected that we should realize an ordered array of uniform quantum wires of ferroelectrics with larger dielectric constant separated by an amorphous SiO<sub>2</sub> wall with lower dielectric constant by filling the mesopores of MCM-41 with BaTiO<sub>3</sub> and SrBi<sub>2</sub>Ta<sub>2</sub>O<sub>9</sub>.

## II. EXPERIMENT

The MCM-41 molecular sieve sample used in this experiment was synthesized from a mixture of SiO<sub>2</sub> 1.00: dodecyltrimethylammonium chloride (C<sub>12</sub> TMAC) 0.70:NaOH 0.24:H<sub>2</sub>O 62.2. The mixture was stirred at room temperature and then heated at 140 °C for 48 h. After washing at 80 °C for 24 h and thermal dehydration at 80 °C for 24 h, the MCM-41 sample was calcinated at 700 °C for 6 h in flowing oxygen to remove the organic molecules incorporated during the templating process from the mesopores.

For preparation of BaTiO<sub>3</sub> mesocrystals the MCM-41 samples were soaked into BaTiO<sub>3</sub> precursor solutions with various concentrations. The solutions of 0.004, 0.04, and 0.1 mol/l were prepared by dissolving barium dihydroxide and titanium tetrachloride in distilled water. After 24 h stirring, the soaked MCM-41 samples were dried in a vacuum and then heated in flowing oxygen at 700 °C for 3 h.

In preparation of SrBi<sub>2</sub>Ta<sub>2</sub>O<sub>9</sub> mesocrystals, the MCM-41 sample soaked in an absolute ethanol solution of strontium oxalate monohydrate, bismuth chloride, and tantalum chloride with a concentration of 0.005 mol/l for 24 h with stirring. The soaked sample was dried and then calcinated in flowing oxygen at 800 °C for 3 h.

X-ray diffraction (XD) patterns of the samples were measured with a Rigaku CN2013 diffractometer using Cu K $\alpha$  radiation. High-resolution transmission electron microscopy (HRTEM) was performed with a JEOL JEF-3000F transmission electron microscope operated at 300 kV for an edge of the samples dispersed on a carbon film. The instrument has a field emission electron source and a resolution of 2 Å. Electron energy loss spectra (EELS) from the area of 10–100 Å diameter of the TEM sample were measured with a Gatan model-666 electron energy analyzer equipped to the JEF-3000F microscope. Ultraviolet-visible diffuse reflectance spectra of the samples were measured with a resolution of 0.002 eV using a JASCO V-550 spectrometer.

<sup>a)</sup>Electronic mail: kohiki@che.kyutech.ac.jp

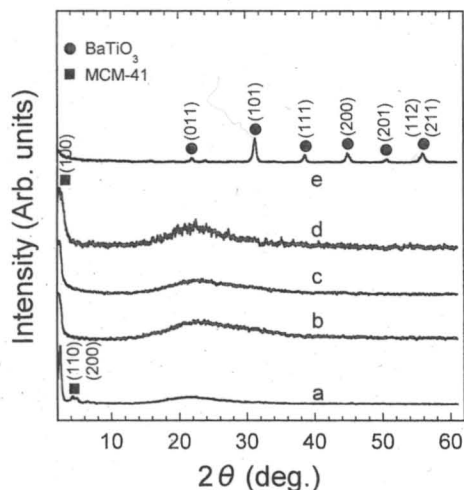


FIG. 1. X-ray diffraction patterns of the MCM-41 (a), the soaked samples with 0.004 (b), 0.04 (c), and 0.1 mol/l (d), all infilled with BaTiO<sub>3</sub> mesocrystals, and the BaTiO<sub>3</sub> particles (e).

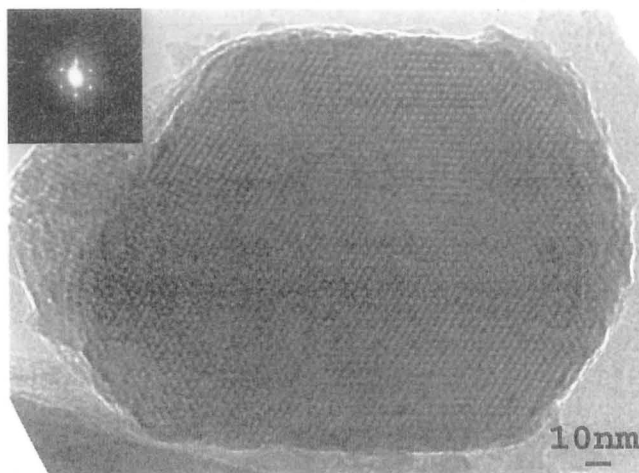
### III. RESULTS AND DISCUSSION

#### A. BaTiO<sub>3</sub> mesocrystals

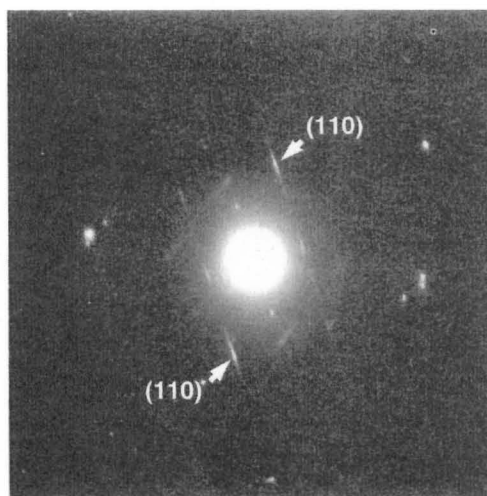
The XD pattern of the MCM-41 sample depicted in Fig. 1(a) can be indexed on a hexagonal unit cell with  $a \sim 39 \text{ \AA}$  ( $a = 2d_{100}\sqrt{3}$  and  $d_{100} = 34 \text{ \AA}$ ). Since the reported wall thickness of the MCM-41 is 8–9 Å,<sup>7</sup> the innerdiameter of the mesopores becomes  $\sim 30 \text{ \AA}$ . XD patterns Figs. 1(b)–1(d) show no peaks from BaTiO<sub>3</sub> crystals. They correspond to BaTiO<sub>3</sub> mesocrystals, respectively, from the 0.004, 0.04, and 0.1 mol/l solutions. BaTiO<sub>3</sub> mesocrystals smaller than 30 Å in the mesopores of MCM-41 cannot preserve the translational symmetry in both intra- and interpores of the MCM-41, and there are no BaTiO<sub>3</sub> particles at the surface of the soaked samples.

A typical XD pattern of crystalline BaTiO<sub>3</sub> shown in Fig. 1(e) was obtained for the powders from the 0.004 mol/l solution. Crystalline size of the powders, 500 Å, was determined from the full width at half maximum (FWHM) of the (101) reflection using Scherrer's equation,<sup>11</sup>  $D = K\lambda / (B \cos \theta)$ , where  $D$  is the crystalline size,  $K$  the Scherrer's constant (on the order of unity for usual crystals<sup>11</sup>),  $\lambda$  is the x-ray wavelength,  $B$  is the FWHM of the diffraction peak, and  $\theta$  is the diffraction angle.

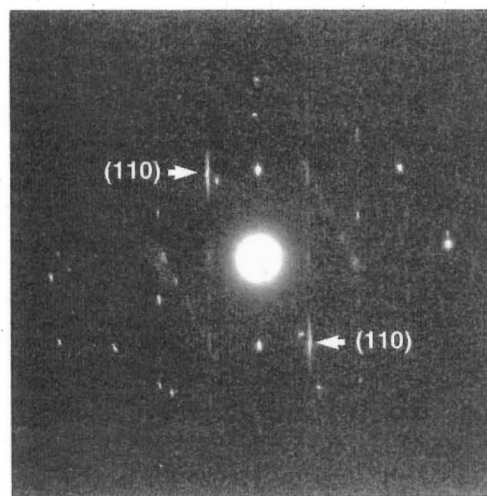
As shown in Fig. 2(a), HRTEM with the beam direction parallel to the pore direction of the MCM-41 revealed that the MCM-41 sample partially contains a smaller pore structure,  $a \sim 36 \text{ \AA}$  ( $d_{100} = 31 \text{ \AA}$ ), than the average one (39 Å) by XD. The ED pattern in the inset of Fig. 2 shows that two-dimensional hexagonal ordering of the pores are preserved perpendicular to the beam direction. ED patterns of the soaked samples without XD peaks are presented in Figs. 2(b) and 2(c), respectively, from the 0.004 and 0.1 mol/l solutions. They show bright spots with a spacing of 2.8 Å, corresponding to the (110) reflection of BaTiO<sub>3</sub> unit cell, on



(a)



(b)



(c)

FIG. 2. (a) Transmission electron micrograph of MCM-41. Inset: Electron diffraction pattern indexed as the  $kh0$  projection of a hexagonal unit cell with  $a \sim 36 \text{ \AA}$ . (b) Electron diffraction pattern of the soaked sample with 0.004 mol/l solution, infilled with BaTiO<sub>3</sub> mesocrystals. (c) Electron diffraction pattern of the soaked sample with 0.1 mol/l solution, infilled with BaTiO<sub>3</sub> mesocrystals.

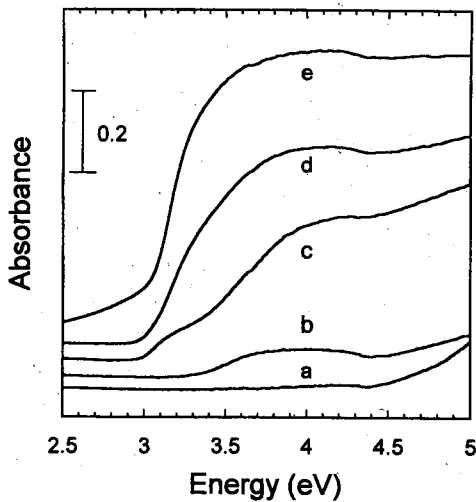


FIG. 3. Ultraviolet-visible diffuse reflectance spectra of the MCM-41 (a), the soaked samples with 0.004 (b), 0.04 (c), and 0.1 mol/l (d), all infilled with BaTiO<sub>3</sub> mesocrystals, and the BaTiO<sub>3</sub> particles (e).

streak lines with the spacing of 3–6 Å. EELS of the soaked sample from the 0.004 mol/l solution showed the same BaM, TiL, and OK loss spectra as those of BaTiO<sub>3</sub> powders. It is expected that the mesopores of MCM-41 are filled with columnar BaTiO<sub>3</sub> mesocrystals and ordered arrays of ferroelectric quantum wires are formed.

Optical absorption spectra of the samples are shown in Fig. 3. The MCM-41 sample showed no absorption edge in the region from 3.0 to 4.5 eV as seen in Fig. 3(a). As shown by the spectra Figs. 3(b)–3(d) of the soaked samples, BaTiO<sub>3</sub> mesocrystals showed blueshifts in the lowest electron transition energy from the filled O 2*p* states to empty Ti 3*d* states. The blueshift is more apparent for the sample soaked in lower concentration solution. The transition, began at 3.0<sub>2</sub> eV for the BaTiO<sub>3</sub> particles, shifted to about 3.3<sub>5</sub> eV for the BaTiO<sub>3</sub> mesocrystals with the 0.004 mol/l solution, presumably due to quantum-confinement effects. The major absorption edge of BaTiO<sub>3</sub> mesocrystals from the 0.04 mol/l solution was at 3.2<sub>5</sub> eV, though the minor absorption began at 3.0<sub>2</sub> eV. The absorption edge of BaTiO<sub>3</sub> mesocrystals from the 0.1 mol/l solution stayed at 3.0<sub>2</sub> eV which coincides to that of bulk BaTiO<sub>3</sub>.

Lowering the concentration of soaking solution enlarged the optical absorption edge of BaTiO<sub>3</sub> mesocrystals. The fact that the absorption edge of mesocrystals from the solution with higher concentration remained at the same energy as for bulk BaTiO<sub>3</sub> is evidence of the inter-pore interaction of quantum-confined BaTiO<sub>3</sub> columns. The concentration dependence in electron transition energy reflects that the inter-pore interaction decreased with increasing distance between the pores filled with BaTiO<sub>3</sub> mesocrystals. The large dielectric constant ( $\epsilon_r \approx 200$ ) and effective electron mass ( $m_e^* = 6.5m_0$ )<sup>12</sup> of BaTiO<sub>3</sub> presumably led to a widely spreading wavefunction of an exciton with an effective Bohr radius,  $a_B^*$ , of approximately 15 Å. Since the wall thickness ( $d \sim 10$  Å) of the MCM-41 is smaller than  $a_B^*$ , the excited electron in a filled pore could transfer to the neighboring

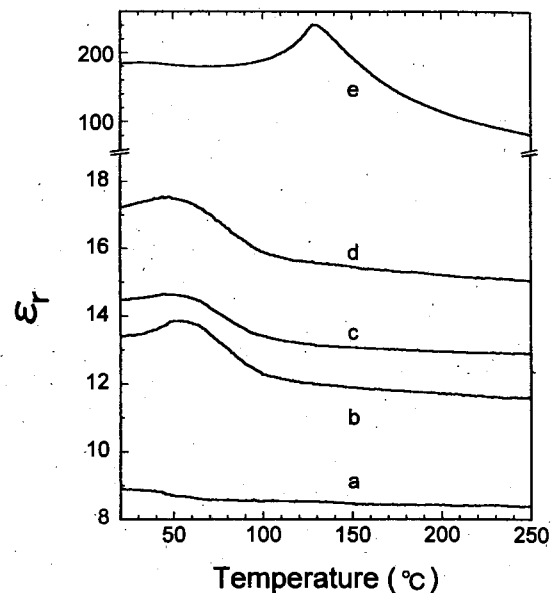


FIG. 4. Temperature dependence of relative dielectric constant of the MCM-41 (a), the soaked samples with 0.004 (b), 0.04 (c), and 0.1 mol/l (d), all infilled with BaTiO<sub>3</sub> mesocrystals, and the BaTiO<sub>3</sub> particles (e).

Dielectric constants of the pelletized samples (MCM-41, soaked samples, and BaTiO<sub>3</sub> particles) were measured in the range from 20 to 250 °C at 100 kHz, and are shown in Fig. 4. The temperature dependence of the dielectric constant of the MCM-41, soaked samples, and BaTiO<sub>3</sub> particles exhibited variations. The MCM-41 [Fig. 4(a)] showed no apparent peak of the dielectric constant. The soaked samples showed an identical dielectric constant maximum at around 55 °C as can be seen in Figs. 4(b)–4(d) notwithstanding there are large differences in concentrations of the soaking solution. As shown in Fig. 4(e), the BaTiO<sub>3</sub> powder exhibited a maximum at around 130 °C. The dielectric constant maximum temperature decreased about 75 °C with decreasing crystalline size from 500 to  $\sim 30$  Å. Lowering the transition temperature is a generally recognized effect of size reduction.

As described above, there was no concentration dependence of the dielectric constant maximum temperature for BaTiO<sub>3</sub> mesocrystals. It is well known that the attractive part of the dipole–dipole interaction potential varies as  $\mu_i \mu_j / R^3$ , where  $\mu_i$  and  $\mu_j$  are the *i*th and *j*th dipole moments and *R* is the distance between the *i* and *j* dipoles. Therefore, the dipole–dipole interaction should disappear over the wall ( $d \sim 10$  Å) of the MCM-41. The dielectric characteristics of the quantum-confined BaTiO<sub>3</sub> columns reflect only the interactions between the dipole moments in mesocrystals. The dielectric characteristic temperature *T* determined from  $\Sigma \mu_i \mu_j / 3kT$ , where *k* is the Boltzmann constant, should be lowered by the decreasing of  $\Sigma \mu_i \mu_j$  in mesocrystals isolated with the low dielectric constant wall of MCM-41.

## B. SrBi<sub>2</sub>Ta<sub>2</sub>O<sub>9</sub> mesocrystals

The XD patterns depicted by Figs. 5(a) and 5(b) correspond to the MCM-41 sample before and after the 800 °C

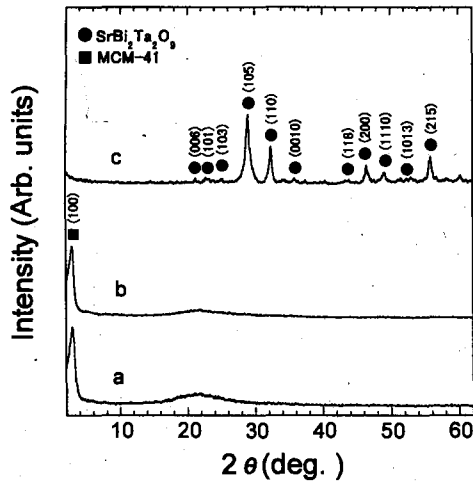


FIG. 5. X-ray diffraction patterns of the MCM-41 calcinated at 700 °C (a), at 800 °C (b), subjected to the same temperature program as for the  $\text{SrBi}_2\text{Ta}_2\text{O}_9$  decomposition, the soaked sample with 0.005 mol/l solution (c), infilled with  $\text{SrBi}_2\text{Ta}_2\text{O}_9$  mesocrystals, and the  $\text{SrBi}_2\text{Ta}_2\text{O}_9$  powders from the solution (d).

though the pores shrank by approximately 8% ( $a \sim 36$  Å). It is well known that calcination at elevated temperature diminishes the pore size due to partial restructuring of the walls. Such restructuring is also manifested by reduced intensity of the (100) reflection due to a loss of the long-range ordering.

The XD pattern [Fig. 5(c)] showed no x-ray diffraction peaks from  $\text{SrBi}_2\text{Ta}_2\text{O}_9$  crystals.  $\text{SrBi}_2\text{Ta}_2\text{O}_9$  mesocrystals smaller than 30 Å cannot preserve translational symmetry in both intra- and interpores of the MCM-41, and there are no  $\text{SrBi}_2\text{Ta}_2\text{O}_9$  particles attached to the soaked sample surface. Powders of  $\text{SrBi}_2\text{Ta}_2\text{O}_9$  obtained from the precursor solution by drying and calcination produced the XD pattern shown in Fig. 5(d). The crystalline size of the powders, 150 Å, was estimated from the FWHM of the (105) reflection using Scherrer's equation.

The optical absorption spectra of the samples are presented in Fig. 6. The MCM-41 sample calcinated at 800 °C also showed no absorption edge below 4.5 eV as can be seen in Fig. 6(a). For the soaked sample, major and minor absorp-

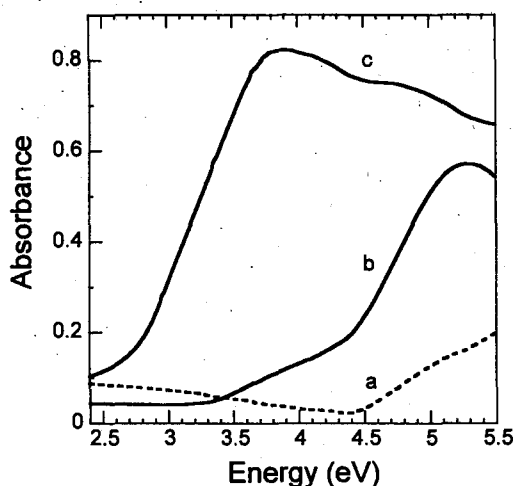


FIG. 6. Optical absorption spectra of the MCM-41 calcinated at 800 °C (a), the soaked sample with 0.005 mol/l solution (b), infilled with  $\text{SrBi}_2\text{Ta}_2\text{O}_9$  mesocrystals, and the  $\text{SrBi}_2\text{Ta}_2\text{O}_9$  powders from the solution (c).

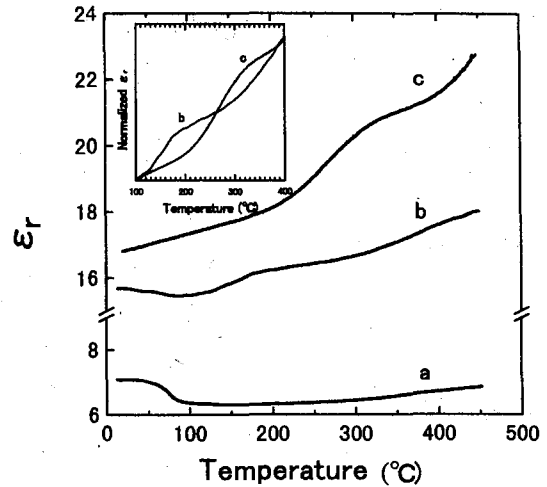


FIG. 7. Temperature dependence of relative dielectric constant of the MCM-41 calcinated at 800 °C (a), the soaked sample with 0.005 mol/l solution (b), infilled with  $\text{SrBi}_2\text{Ta}_2\text{O}_9$  mesocrystals, and the  $\text{SrBi}_2\text{Ta}_2\text{O}_9$  powders from the solution (c). Inset: Normalized relative dielectric constant at from 100 to 400 °C.

tion edges were observed at around 4.1<sub>8</sub> and 3.3<sub>2</sub> eV, respectively, as depicted in Fig. 6(b). The absorption edge of the  $\text{SrBi}_2\text{Ta}_2\text{O}_9$  powders was 2.7<sub>0</sub> eV as shown by Fig. 6(c). The increase of about 1.4 eV in the electron transition energy for the pore-filled mesocrystals smaller than 30 Å from the powders with crystalline size of 150 Å is evidence of the quantum confinement of the  $\text{SrBi}_2\text{Ta}_2\text{O}_9$ . The larger shift observed for  $\text{SrBi}_2\text{Ta}_2\text{O}_9$  compared to  $\text{BaTiO}_3$  is ascribed to the smaller dielectric constant of  $\text{SrBi}_2\text{Ta}_2\text{O}_9$  ( $\epsilon_r \approx 20$ ) compared with that of  $\text{BaTiO}_3$  ( $\epsilon_r \approx 200$ ). The small dielectric constant causes confinement of the exciton wave function of  $\text{SrBi}_2\text{Ta}_2\text{O}_9$  mesocrystals in the pores of the MCM-41.

Tight-binding calculations for the  $\text{SrBi}_2\text{Ta}_2\text{O}_9$  crystal revealed that the valence band maximum (VBM) at  $\Gamma$  arises from  $O p$  and some  $Bi s$  states, while the conduction band minimum (CBM) at  $M$  consisted of  $Bi p$  states followed by  $Ta d$  states.<sup>13</sup> Both the VBM and CBM are states localized in the  $\text{Bi}_2\text{O}_2$  layer. The observed blueshift of the optical absorption peak reflects a quantum-confined effect on the energy dispersion of the band electrons, especially those localized in the  $\text{Bi}_2\text{O}_2$  layer. In  $\text{SrBi}_2\text{Ta}_2\text{O}_9$  the perovskite blocks of  $\text{Sr-Ta-O}$  are primarily responsible for the ferroelectricity, and the layers of  $\text{Bi}_2\text{O}_2$  are amplifying the ferroelectric dipole. A displacement of  $Ta$  in the perovskite block should be affected by the confinement as should  $Bi$  in the  $\text{Bi}_2\text{O}_2$  layer. In mesocrystals forming quantum wires in the pores of MCM-41, displacement restrictions for the  $Ta-O$  bond in the  $ab$  plane and those for the  $Bi-O$  bond should result in a prominent deterioration of dielectric properties.

The dielectric constants of the pelletized samples (MCM-41 sample, soaked sample, and  $\text{SrBi}_2\text{Ta}_2\text{O}_9$  powders) were measured in the range from 20 to 450 °C at 100 kHz, and are shown in Fig. 7. The temperature dependencies of the dielectric constants of the MCM-41 sample, soaked sample, and  $\text{SrBi}_2\text{Ta}_2\text{O}_9$  powders were different from each other. From 100 to 400 °C the MCM-41 sample showed no peaks in the dielectric constant lying at low level ( $\epsilon_r \approx 7$ ). As shown in the inset of Fig. 7, the soaked sample showed a

dielectric constant maximum at around 180 °C, largely different from that of the SrBi<sub>2</sub>Ta<sub>2</sub>O<sub>9</sub> powders which show a maximum at around 320 °C. The dielectric constant maximum temperature dropped about 140 °C with decrease of the crystalline size from 150 to ~30 Å. The observed decrease in the dielectric constant maximum temperature was larger for SrBi<sub>2</sub>Ta<sub>2</sub>O<sub>9</sub> mesocrystals (approximately 1.2 °C/Å) than for BaTiO<sub>3</sub> mesocrystals (approximately 0.16 °C/Å). As described for BaTiO<sub>3</sub>, the dielectric characteristics of mesocrystals reflect only the intrapore interactions between the dipole moments in quantum-confined ferroelectric columns. For SrBi<sub>2</sub>Ta<sub>2</sub>O<sub>9</sub> mesocrystals, the effects should be more prominent due to stronger confinement than for BaTiO<sub>3</sub> mesocrystals.

#### IV. SUMMARY

We have demonstrated quantum-confinement effects on the optical and dielectric properties for mesocrystals  $\leq 30$  Å of BaTiO<sub>3</sub> and SrBi<sub>2</sub>Ta<sub>2</sub>O<sub>9</sub>. BaTiO<sub>3</sub> mesocrystals showed a blueshift in the optical band gap from 3.0<sub>2</sub> to 3.3<sub>5</sub> eV, and a decrease in the dielectric constant maximum temperature from 130 to 55 °C. SrBi<sub>2</sub>Ta<sub>2</sub>O<sub>9</sub> mesocrystals also showed an increase in the optical band gap from 2.7<sub>0</sub> to 4.1<sub>8</sub> eV, and a decrease in the dielectric constant maximum temperature

from 320 to 180 °C. The observed optical and dielectric quantum-confinement effects generally agree with the recognized consequence of reduced size. The larger effects for SrBi<sub>2</sub>Ta<sub>2</sub>O<sub>9</sub> mesocrystals than for BaTiO<sub>3</sub> mesocrystals may be due to the smaller dielectric constant and anisotropic crystal structure of SrBi<sub>2</sub>Ta<sub>2</sub>O<sub>9</sub>.

- <sup>1</sup>D. McCauley, R. E. Newnham, and C. A. Randall, *J. Am. Ceram. Soc.* **81**, 979 (1998).
- <sup>2</sup>A. Shaikh, R. Vest, and G. Vest, *IEEE Trans. Ultrason. Ferroelectr. Freq. Control* **36**, 407 (1990).
- <sup>3</sup>S. Schlag and H. F. Eicke, *Langmuir* **10**, 3357 (1994).
- <sup>4</sup>J. U. Müller and K. Barner, *Ferroelectrics* **108**, 83 (1990).
- <sup>5</sup>M. Anliker, H. R. Brugger, and T. Känzig, *Helv. Phys. Acta* **27**, 99 (1954).
- <sup>6</sup>K. Uchino, E. Sadanaga, and T. Hirose, *J. Am. Ceram. Soc.* **72**, 1555 (1989).
- <sup>7</sup>For example, C. T. Kresge, M. E. Leonowicz, W. J. Roth, J. C. Vartuli, and J. S. Beck, *Nature (London)* **359**, 710 (1992).
- <sup>8</sup>R. G. Rhodes, *Acta Crystallogr.* **4**, 105 (1951).
- <sup>9</sup>C. A. Paz de Araujo, J. D. Cuchiaro, L. D. McMillan, M. C. Scott, and J. F. Scott, *Nature (London)* **374**, 627 (1995).
- <sup>10</sup>E. C. Subbarao, *J. Am. Ceram. Soc.* **45**, 166 (1962).
- <sup>11</sup>L. S. Birks and H. Friedman, *J. Appl. Phys.* **17**, 687 (1946).
- <sup>12</sup>C. N. Berglund and W. S. Bear, *Phys. Rev.* **157**, 358 (1967).
- <sup>13</sup>J. Robertson, C. W. Chen, W. L. Warren, and C. D. Gutelben, *Appl. Phys. Lett.* **69**, 1704 (1996).